Molecular influence on nuclear-quadrupole-coupling effects in laser induced alignment ⊘

Special Collection: Molecular Dynamics, Methods and Applications 60 Years after Rahman

Linda V. Thesing; Andrey Yachmenev (iD) ; Rosario González-Férez (iD) ; Jochen Küpper ✉ (iD)

⟳ Check for updates

View Online   Export Citation

Articles You May Be Interested In

Role of rotational temperature in adiabatic molecular alignment

J. Chem. Phys. (November 2006)

Strongly aligned molecules inside helium droplets in the near-adiabatic regime

J. Chem. Phys. (June 2017)

Ab initio study of the electronic structure of the crystalline high-mobility organic semiconductor 1,4-diiodobenzene

J. Chem. Phys. (August 2006)

Molecular influence on nuclear-quadrupole-coupling effects in laser induced alignment

View Online   Export Citation   CrossMark

Linda V. Thesing,[1,2,3] Andrey Yachmenev,[1,2,a] Rosario González-Férez,[4,b] and Jochen Küpper[1,2,3,c]

AFFILIATIONS

[1] Center for Free-Electron Laser Science CFEL, Deutsches Elektronen-Synchrotron DESY, Notkestrasse 85,
22607 Hamburg, Germany
[2] Center for Ultrafast Imaging, Universität Hamburg, Luruper Chaussee 149, 22761 Hamburg, Germany
[3] Department of Physics, Universität Hamburg, Luruper Chaussee 149, 22761 Hamburg, Germany
[4] Instituto Carlos I de Física Teórica y Computacional and Departamento de Física Atómica, Molecular y Nuclear,
Universidad de Granada, 18071 Granada, Spain

Note: This paper is part of the JCP Special Topic on Molecular Dynamics, Methods and Applications 60 Years After Rahman.
[a] Electronic mail: andrey.yachmenev@cfel.de
[b] Electronic mail: rogonzal@ugr.es
[c] Author to whom correspondence should be addressed: jochen.kuepper@cfel.de.
https://www.controlled-molecule-imaging.org

ABSTRACT

We computationally studied the effect of nuclear-quadrupole interactions on the field-free impulsive alignment of different asymmetric-top molecules. Our analysis is focused on the influence of the hyperfine- and rotational-energy-level structures. These depend on the number of nuclear spins, the rotational constants, and the symmetry of the tensors involved in the nuclear spin and external field interactions. Comparing the prototypical large-nuclear-spin molecules iodobenzene, 1,2-diiodobenzene, 1,3-diiodobenzene, and 2,5-diiodobenzonitrile, we demonstrate that the magnitude of the hyperfine splittings compared to the rotational-energy splittings plays a crucial role in the spin-rotational dynamics after the laser pulse. Moreover, we point out that the impact of the quadrupole coupling on the rotational dynamics decreases when highly excited rotational states dominate the dynamics.

I. INTRODUCTION

The coupling of rotational and nuclear spin angular momenta, known as hyperfine interaction, can have a significant influence on the rotational dynamics of molecules and is at the core of the nuclear magnetic resonance measurement.[1–9] There are several mechanisms of hyperfine interaction; the most prominent is the nuclear-quadrupole coupling. This occurs in molecules containing nuclei with partly filled shells, resulting in non-spherical nuclear shapes and the appearance of an electric nuclear quadrupole moment. This quadrupole couple electrostatically interacts with the field gradient induced by other moving charged particles in the molecule, i.e., the nuclei and electrons.

Generally, nuclear-quadrupole coupling is strong in molecules containing heavy atoms, such as Se, Br, I, Fe, Au, or Pt, which are

also found in many biologically relevant molecules. Due to their very large x-ray- and electron-scattering cross sections, these atoms are often chemically attached to molecular compounds and used as marker atoms in diffractive imaging experiments.[10–13] Furthermore, in Coulomb-explosion imaging, these heavy atoms often show good axial recoil, enabling the observation of molecular orientation and internal structure during dynamical processes.[14–16]

An indispensable component of high-resolution imaging experiments is the laser-induced alignment of molecules, enabling measurements to be performed in the molecule-fixed frame without orientation averaging. To avoid perturbations due to the presence of external fields, alignment under field-free conditions is often favorable. Field-free alignment relies on the preparation of rotational wave packets by means of intense optical laser pulses.[17,18] Since the wave packets are in non-stationary states, they dephase and rephase

periodically, changing the alignment with time, even after the pulsed excitation. Typical pulse shapes range from short kick pulses[19–21] to pulses with long rising and short falling edges.[22–26] The time-evolution of the molecular alignment in field-free conditions is a revival structure, ideally with nearly the same degree of alignment appearing every rotational period. The latter is, however, only valid for molecules with regular spacings between the rotational energy levels, such as rigid linear and symmetric top molecules.

The revivals of molecular alignment are highly sensitive to the molecule's rotational energy level structure. A detailed understanding of various molecular degrees of freedom that can couple to rotations is thus needed to accurately predict the alignment dynamics of molecules. It is well established that hyperfine interactions can have a significant impact on the rotational dynamics of molecules prepared in single rotational states.[9] Furthermore, experimental evidence of the influence of nuclear quadrupole effects on the impulsive alignment dynamics was published recently for I_2 molecules.[27] In computational studies of linear and asymmetric top molecules, we found a nontrivial dependence of the nuclear quadrupole effects on the intensity of the laser field.[28,29]

Here, we provide deeper insight into the effect of the quadrupole coupling on the alignment for different molecular species. We compared the results across asymmetric top molecules with different numbers of nuclear quadrupolar nuclei, their different positions in the molecule, and different molecular symmetries. Our molecular set contains C_{2v}-symmetric molecules with one and two iodine atoms, i.e., iodobenzene and the 1,2- and 1,3-isomers of diiodobenzene, besides the already investigated 1,4-isomer and the C_s-symmetric molecules diiodobenzonitrile and 1,3-bromoiodobenzene. In addition, we consider a hypothetical modified single-spin 1,3-diiodobenzene.

We focus on the short-pulse-alignment dynamics, as our previous results showed that the influence of the nuclear-quadrupole coupling on adiabatic alignment is negligible for similar molecules.[29] First, we summarize our theoretical approach in Sec. II. We then present impulsive alignment results for low- (Sec. III A) and high-intensity (Sec. III B) laser pulses for a rotational temperature of $T_{rot} = 0$ K. Finally, we analyze the rotational dynamics of cold thermal ensembles and individual excited states.

II. THEORETICAL DESCRIPTION

We studied the laser-induced rotational dynamics of asymmetric top molecules, taking into account the nuclear-quadrupole interactions.[28] The field-free spin-rotational Hamiltonian of the system is given by

$$\hat{H}_{mol} = \hat{H}_{rot} + \sum_l \mathbf{V}(l) \cdot \mathbf{Q}(l), \quad (1)$$

where $\hat{H}_{rot} = A\hat{J}_a^2 + B\hat{J}_b^2 + C\hat{J}_c^2$ is the rigid-rotor Hamiltonian with the rotational constants A, B, C and the components $\hat{J}_i$, $i = a, b, c$, of the rotational angular momentum operator $\hat{\mathbf{J}}$. The second term in the Hamiltonian (1) describes the interaction of the quadrupole-moment tensor $\mathbf{Q}(l)$ of the lth nucleus with the electric-field-gradient (EFG) tensor $\mathbf{V}(l)$. The sum runs over all nuclei with significant quadrupole moments l in the molecule.

The polarizability interaction with the nonresonant laser field, linearly polarized along the laboratory-fixed Z axis, can be written as

$$\hat{H}_{las}(t) = -\frac{I(t)}{2\varepsilon_0 c}\alpha_{ZZ}, \quad (2)$$

where $I(t)$ is the intensity of the laser field and α_{ZZ} is the corresponding element of the molecule's polarizability tensor in the laboratory-fixed frame.

The geometrical structures, principal axes of inertia, and most-polarizable (MPA) axes of iodobenzene (IB), diiodobenzonitrile (DIBN), 1,3-diiodobenzene (1,3-DIB), and 1,2-diiodobenzene (1,2-DIB) are shown in Fig. 1. All four molecules contain one or two ^{127}I nuclei, which produce considerably large hyperfine energy splittings of the rotational states due to iodine's large quadrupole moment $eQ = -696$ mb.[30] The IB molecule has only one iodine nucleus, and the total-nuclear-spin angular momentum is $\hat{\mathbf{I}} = \hat{\mathbf{I}}_1$, where $I_1 = 5/2$. For the molecules with two iodine nuclei, $\hat{\mathbf{I}} = \hat{\mathbf{I}}_1 + \hat{\mathbf{I}}_2$, the associated quantum number can have values $I = 0, \ldots, 5$. The total angular momentum is given by $\hat{\mathbf{F}} = \hat{\mathbf{J}} + \hat{\mathbf{I}}$. The nitrogen nucleus in DIBN has an additional nonzero quadrupole moment $eQ = 20.44$ mb,[30] which is, however, relatively small compared to iodine and, therefore, neglected for the purpose of this study. This could also be achieved by the ^{15}N isotopologue with spin 1/2 and, therefore, $eQ = 0$. For 1,3-bromoiodobenzene (1,3-BIB), we assume two different quadrupole-coupled nuclei, ^{127}I and ^{79}Br, the more abundant isotope of bromine with $Q = 313$ mb.[30] All important parameters for the molecules in this study, such as rotational constants, polarizability, and EFG tensor elements, are listed in Appendix A.

The simulations of the spin-rotational dynamics of molecules subject to external electric fields were performed using the variational approach Richmol[28,31] and the same computational setup as
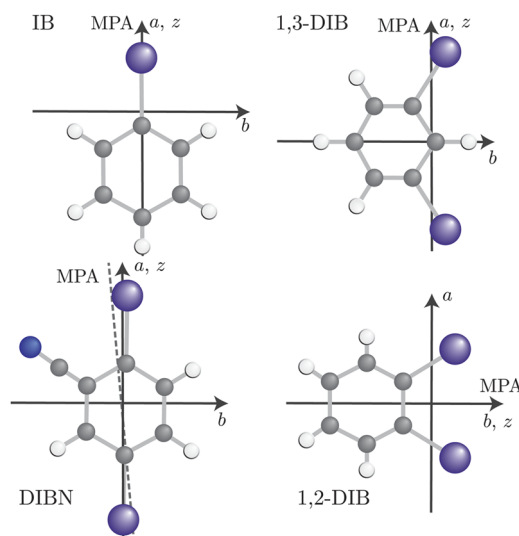

FIG. 1. Sketches of the molecules IB, DIBN, 1,3-DIB, and 1,2-DIB. For IB and 1,3-DIBN the most polarizable axis (MPA) is parallel to the a axis, for DIBN it forms an angle of 5° with the a axis, and for 1,2-DIB the MPA is parallel to the b axis. The molecule-fixed z axis is indicated in the respective sketches.

described in our previous work.[29] The total Hamiltonian is composed of the sum $\hat{H}_{mol} + \hat{H}_{las}$, and the total time-dependent wave function is expanded on the basis of eigenfunctions $|F, \tilde{J}_{\tilde{K}_a \tilde{K}_c}, n, M\rangle$ of the field-free time-independent Hamiltonian $\hat{H}_{mol}$. The details of the functional form of these basis functions are described in Appendix B. The alignment of the molecules is quantified by the expectation value $\langle \cos^2 \theta \rangle$, where θ is the angle between the laser polarization axis and the MPA of the molecule. In the present setup, the laser polarization is aligned along the laboratory-fixed Z axis, and the MPA of all molecules is strictly or nearly parallel to one of the principal axes of inertia (see Fig. 1). This simplifies calculations of the expectation value $\langle \cos^2 \theta \rangle$ since the θ angle can be associated with the corresponding Euler angle.

We compared the post-pulse molecular alignment with and without the nuclear-quadrupole-coupling term in (1) for initial rotational temperatures $T_{rot} = 0, 0.1$, and 0.3 K. We used the eigenstates of $\hat{H}_{mol}$ and $\hat{H}_{rot}$ as initial field-free molecular states in the calculations with and without quadrupole coupling, respectively. We assumed equal populations for all hyperfine components of a single rotational state, mimicking experimental conditions in molecular beams, where nuclear-spin states typically do not cool and nuclear-spin temperatures correspond to the high-temperature limit before expansion. Therefore, even for rotational temperatures $T_{rot} = 0$ K, the alignment was calculated by averaging over the results of independent calculations for every hyperfine component of the ground rotational state $J = 0$. For the finite-temperature calculations, further averaging was performed by Boltzmann weighting the rotational states.

III. RESULTS AND DISCUSSION

A. Low-intensity impulsive alignment

Previously, we found that the effect of the nuclear-quadrupole coupling strongly depends on the laser intensity and is larger at a lower intensity.[28,29] Therefore, we begin by analyzing the influence of the quadrupole coupling on the impulsive alignment induced by a 1 ps (FWHM) Gaussian laser pulse with a moderate peak intensity $I_0 = 10^{11}$ W/cm^2. Figure 2 shows the temporal evolution of the post-pulse alignment dynamics, characterized by $\langle \cos^2 \theta \rangle(t)$, computed for different molecules at $T_{rot} = 0$ K. The results including nuclear-quadrupole coupling are plotted with thick lines and the results of rigid-rotor calculations, i.e., neglecting the nuclear-quadrupole coupling, are plotted with thin black lines.

In the rigid-rotor case, the alignment revival structures in Fig. 2 look fairly regular for all molecules, which is the result of dephasing and rephasing of rather narrow rotational wave packets. The revivals change from one molecule to another due to their distinct rotational-energy-level structures and, to some extent, due to slightly different interaction strengths with the laser field caused by the different polarizabilities. Due to the weak intensity of the field, the post-pulse dynamics of IB, DIBN, and 1,3-DIB is dominated by the coherences between the low-energy rotational states with $K_a = 0$. K_a is the quantum number of the rotational angular momentum projection operator onto the molecule-fixed a axis. Since the energies of these states look fairly similar to the energy levels of a symmetric top, the revival patterns in Figs. 2(a)–2(c) repeat themselves after multiples of the respective rotational periods $\tau_{rot}^{IB} = 707.69$ ps,
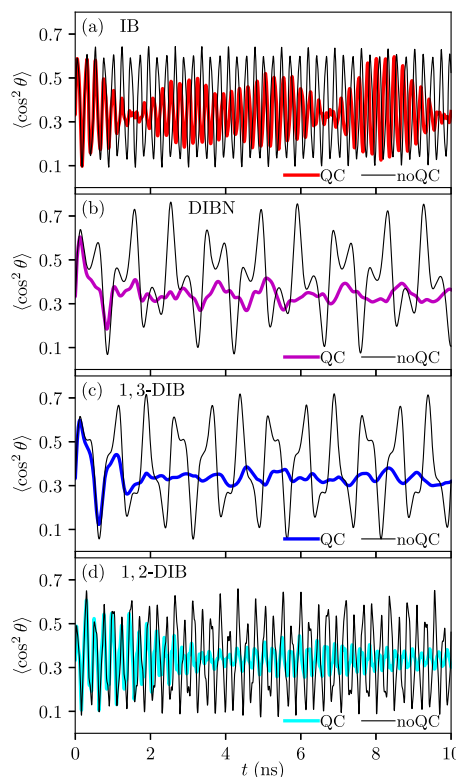

FIG. 2. Impulsive alignment induced by a Gaussian laser pulse with $\tau_{FWHM} = 1$ ps and $I_0 = 10^{11}$ W/cm^2 for (a) IB, (b) DIBN, (c) 1,3-DIB, and (d) 1,2-DIB, including (QC), and neglecting the nuclear-quadrupole coupling (noQC).

$\tau_{rot}^{DIBN} = 3365.7$ ps, and $\tau_{rot}^{1,3-DIB} = 2499.4$ ps, with $\tau_{rot} = 1/(B + C)$. In the case of 1,2-DIB, the post-pulse dynamics [Fig. 2(d)] does not show such a periodic behavior due to the molecule's larger rotational asymmetry (see Table I).

The nuclear-quadrupole coupling increases the complexity of the post-pulse alignment dynamics. At early times, the laser pulse $\langle \cos^2 \theta \rangle$ does not show any significant deviation from the rigid-rotor dynamics as the quadrupole coupling is much weaker than the polarizability interaction with the laser field. However, the wavepackets quickly dephase,[29] characteristic of the non-regular hyperfine splittings of low-energy rotational states that dominate the dynamics. Each rotational state of the IB molecule is split into six hyperfine components, at most, while for the molecules with two iodine nuclei, each state has up to 36 hyperfine components. The influence of the quadrupole coupling is noticeably stronger for DIBN and 1,3-DIB molecules [see Figs. 2(b) and 2(c)]. This is due to the rather small B and C rotational constants for these molecules, corresponding rotational-level spacings in DIBN and 1,3-DIB at low rotational excitations that are comparable to or even smaller than the hyperfine splittings. This yields strong mixing of different rotational levels, even in the initial field-free states, giving rise to large dephasing effects. A similar behavior was observed previously for 1,4-DIB.[29] For IB and 1,2-DIB, the hyperfine splittings are much smaller than the rotational level spacings and, therefore, the dephasing effect is weaker. Consequently, the alignment for these

TABLE I. Rotational constants A, B, C, asymmetry parameter κ, elements of the polarizability tensors α_{ij} and electric field gradient tensors $V_{ij}(l)$ of the lth nucleus in the coordinate system defined by the principle axes of inertia. In the case of 1,3-BIB, $V_{ij}(1)$ and $V_{ij}(2)$ refer to the EFG of the iodine and bromine nuclei, respectively. For IB, the experimentally determined rotational constants from Ref. 47, the polarizability tensor from Ref. 37, and the quadrupole-coupling constants from Ref. 47 (Table VI) were used.

	IB	DIBN	1,3-DIB	1,2-DIB	1,3-BIB
A (MHz)	5669.131	1608.324	1859.912	822.0850	2040.244
B (MHz)	750.414293	155.402	210.776	522.1492	281.807
C (MHz)	662.636146	141.709	189.321	319.3276	247.607
κ	−0.965	−0.981	−0.974	−0.193	−0.962
α_{aa} (Å^3)	21.5	34.506	28.847	22.072	25.774
α_{bb} (Å^3)	15.3	21.662	19.789	24.830	18.234
α_{cc} (Å^3)	10.2	12.123	11.292	11.103	10.192
α_{ab} (Å^3)	0	−1.209	0	0	−0.419
$V_{aa}(1)$ (a.u.)	−1892.039/eQ	12.327	7.34	−0.30	8.3735
$V_{bb}(1)$ (a.u.)	978.816/eQ	−6.6802	−1.73	5.88	−2.7590
$V_{cc}(1)$ (a.u.)	913.222/eQ	−5.6472	−5.61	−5.57	−5.6146
$V_{ab}(1)$ (a.u.)	0	1.5092	−7.85	8.84	−7.1745
$V_{aa}(2)$ (a.u.)	0	12.155	7.34	−0.30	4.1656
$V_{bb}(2)$ (a.u.)	0	−6.4317	−1.73	5.88	−0.4784
$V_{cc}(2)$ (a.u.)	0	−5.7230	−5.61	−5.57	−3.6872
$V_{ab}(2)$ (a.u.)	0	0.57071	7.85	−8.84	5.6800

molecules oscillates at frequencies similar to the rigid-rotor results [see Figs. 2(a) and 2(d)]. The effect of the quadrupole coupling is, however, visible in the strongly modified amplitude of the degree of alignment.

In order to illustrate the interplay between the hyperfine-split and the pure rotational energy level spacings, we computed the fast-Fourier transforms (FFTs) of $\langle \cos^2 \theta \rangle(t)$ for IB and 1,3-DIB molecules (see Fig. 3). Here, the wavepackets obtained from the
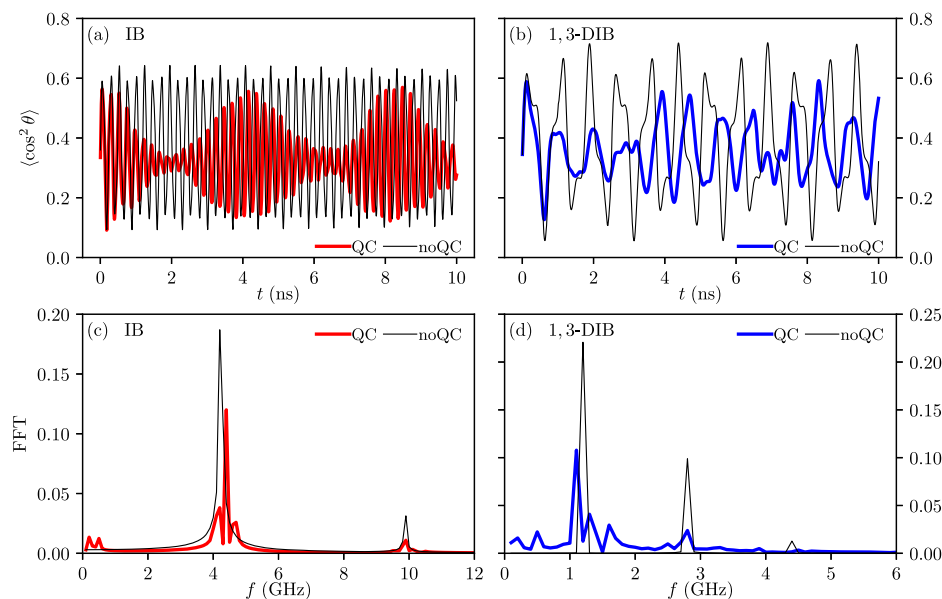
FIG. 3. Impulsive-alignment dynamics for $I_0 = 10^{11}$ W/cm^2 with nuclear-quadrupole coupling (QC) for the initial states (a) $|5/2, 0_{00}, 1/2\rangle$ of IB and (b) $|0, 0_{00}, 0\rangle$ of 1,3-DIB and without the coupling (noQC). (c) and (d) Fast-Fourier transforms of $\langle \cos^2 \theta \rangle$ with and without quadrupole coupling.

single initial hyperfine state $\left|F, \tilde{J}_{\tilde{K}_a \tilde{K}_c}, n, M\right\rangle = \left|5/2, 0_{00}, 1, 1/2\right\rangle$ for IB or $\left|0, 0_{00}, 1, 0\right\rangle$ for 1,3-DIB were analyzed.

The Fourier transforms of the rigid-rotor results show only a few quasi-regularly spaced peaks, reflecting the periodic behavior of $\langle\cos^2\theta\rangle$. For both molecules, the highest intensity peak corresponds to the coupling of the rigid-rotor states $\left|J_{K_a, K_c}\right\rangle = \left|0_{00}, 0\right\rangle$ and $\left|2_{02}, 0\right\rangle$. When the quadrupole coupling is considered, the main rigid-rotor peaks are split into several frequencies corresponding to transitions between different hyperfine states. For IB, Fig. 3(c), the main peak at $f \approx 4.2$ GHz is shifted toward higher frequency, which leads to a faster oscillation of the alignment than for the rigid-rotor, with the opposite effect observed for the main peak $f \approx 1.2$ GHz in 1,3-DIB, Fig. 3(d). The absolute value of the shift is similar for both molecules; however, relative to the peak frequency, the shift in 1,3-DIB is about four times bigger than in IB. Therefore, for 1,3-DIB, the deviations between the phases in the post-pulse alignment for the result with and without the quadrupole coupling occur on the timescale of the rotational revivals. In contrast for IB, the effect is slower than the molecule's longer rotational period. Furthermore, the larger number of hyperfine states in 1,3-DIB compared to IB led to an increased amount of irregularly spaced frequency contributions, giving rise to the non-periodic dynamics [see Fig. 3(b)].

Other initial spin-rotational eigenstates of 1,3-DIB, which contribute to the alignment in Fig. 2(c), show analogous patterns but with different frequency contributions. As a result, the revivals of $\langle\cos^2\theta\rangle$ are on average almost entirely suppressed in 1,3-DIB. For both molecules, the frequency components below $f \approx 1$ GHz originate from the energy gaps between different hyperfine states belonging to the same rotational level, i.e., to pure hyperfine-level population transfers similar to the transitions observed in NMR spectroscopy.

1. Influence of the number and strengths of nuclear spins

To gain more insight into the influence of the number of nuclear spins, we compared the alignment dynamics of 1,3-DIB to that of a modified single-spin 1,3-DIB molecule, where we considered the quadrupole coupling of only one iodine nucleus with all
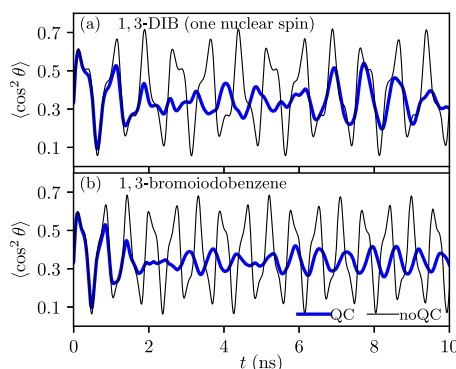

FIG. 4. Impulsive alignment induced by $\tau_{\text{FWHM}} = 1$ ps laser pulses with $I_0 = 10^{11}$ W/cm² for (a) 1,3-DIB neglecting the quadrupole coupling of the second iodine nucleus and (b) 1,3-bromoiodobenzene including (QC) and neglecting the nuclear quadrupole coupling (noQC).

other properties of 1,3-DIB unchanged. This allowed us to compare two molecular systems that differ only in the number of quadrupole-coupled nuclei. Furthermore, we investigated the alignment of 1,3-BIB, which can be considered an intermediate case between 1,3-DIB and the single-spin 1,3-DIB with respect to its rotational and hyperfine splittings.

The alignment of the single-spin 1,3-DIB, shown in Fig. 4(a), exhibits stronger or longer-lasting revivals than the regular 1,3-DIB with two coupled iodine nuclei [see Fig. 2(c)]. When compared to a molecule with the same number of spins, IB, the impact of the quadrupole coupling in the single-spin 1,3-DIB is still more pronounced, Fig. 2(a), even though the quadrupole splittings for both molecules have similar values. However, the pure rotational energy spacings in IB are much larger than in 1,3-DIB. This highlights that it is the relative differences between the hyperfine and the pure rotational energy spacings in the molecule that determines the magnitude of the nuclear-quadrupole effect in the alignment. This conclusion is further supported by the rotational dynamics of 1,2-DIB, which has two iodine nuclei but much larger rotational energy splittings than 1,3-DIB. As a result, $\langle\cos^2\theta\rangle$ is affected by the quadrupole interactions in a manner that qualitatively resembles the behavior of IB rather than 1,3-DIB. This can be seen, for example, when the peak alignment in 1,2-DIB increases after four nanoseconds in Fig. 2(d). The alignment for 1,3-BIB with and without quadrupole coupling is depicted in Fig. 4(b). This molecule has fewer hyperfine energy levels and slightly larger rotational-energy spacings than 1,3-DIB. As a result, the low-amplitude oscillations of the alignment have a more regular structure for 1,3-BIB, while the overall effect of the quadrupole coupling in 1,3-BIB is similar to that in 1,3-DIB; see Fig. 2(c).

2. Influence of the geometric symmetry

Apart from their rotational constants and the number of hyperfine levels, an important distinction of the molecules considered here lies in the symmetry of their EFG and polarizability tensors. In IB, both tensors are diagonal in the coordinate system defined by the principal axes of inertia, while the EFG tensors of the other molecules and the polarizability tensor of DIBN have nonzero off-diagonal elements in the inertial frame. The diagonal elements of these tensors couple rotational states having the same symmetry in the D_2 rotation group.[32] The off-diagonal elements α_{ab} and V_{ab} couple rotational states with $A \leftrightarrow B_c$ symmetry as well as $B_a \leftrightarrow B_b$. For DIBN and the two diiodobenzene molecules, however, a given spin-rotational eigenstate is a linear combination of basis states $\left|F, J_{K_a K_c}, I, M\right\rangle$ with A and B_c or B_a and B_b rotational symmetries. For an eigenstate $\left|F, \tilde{J}_{\tilde{K}_a \tilde{K}_c}, n, M\right\rangle$, only an approximate rotational symmetry can be assigned according to even or odd $\tilde{K}_a$ and $\tilde{K}_c$.[32] Consequently, weak laser-interaction coupling can be observed between the hyperfine states corresponding to rotational states, which are not coupled by the laser field in the absence of the quadrupole interactions.

Without quadrupole interactions, the wave packets of IB, 1,3-DIB, and 1,2-DIB consist exclusively of rotational states of the same symmetry in the D_2 group as the initial state, i.e., A symmetry for $T_{\text{rot}} = 0$ K. For DIBN, states with B_c symmetry also contribute due to the polarizability tensor's nonzero off-diagonal elements. When considering quadrupole coupling, nonzero populations of B_c rotational states are also observed for 1,3-DIB and 1,2-DIB. These

contributions are small, $\lesssim 5\%$, for the initial states and laser intensity considered here and, therefore, do not influence the alignment significantly. However, this aspect of the rotational dynamics is not captured if the nuclear-quadrupole interactions are neglected. In addition, for rotational levels, which are strongly mixed by these interactions, a much larger impact on the population distribution is possible. This is, for instance, the case for the excited states $|2_{12}, M_J\rangle$ and $|2_{02}, M_J\rangle$ of 1,2-DIB [see Sec. III C].

B. High-intensity impulsive alignment

Typical impulsive alignment experiments employ intenser laser pulses,[33–36] which excite a larger number of high-energy rotational states than discussed in Sec. III A. We investigated the strong field alignment using the same pulse shape as in Sec. III A, but with the peak intensity increased tenfold, i.e., $I_0 = 10^{12}$ W/cm^2. The temporal evolution of $\langle \cos^2 \theta \rangle$ for all molecules except 1,2-DIB is characterized by J-type revivals[34,37] that appear at multiples of the rotational periods as well as integer fractions thereof [see Fig. 5]. These beatings originate from the interference of highly excited rotational states with $\Delta K_a = 0$. The asymmetry splittings of these states prevent a complete rephasing of the wave packet, and the peak alignment at the revivals decreases over time.[38]

For 1,2-DIB, we observe clear revival features of a different type spaced by 304 ps in Fig. 5(d). The post-pulse dynamics of this

FIG. 5. Impulsive alignment induced by a Gaussian laser pulse with $\tau_{\text{FWHM}} = 1$ ps and $I_0 = 10^{12}$ W/cm^2 for (a) IB, (b) DIBN, (c) 1,3-DIB, and (d) 1,2-DIB, including (QC), and neglecting the nuclear-quadrupole coupling (noQC).

molecule is dominated by the dephasing and rephasing of rotational states with $\Delta J = \Delta K_a = 2$ and $J \approx K_a$. For large J, the energies of these states can be approximated by $E(J, K_a) \approx \overline{B}J(J+1) + (A - \overline{B})K_a^2$ with $\overline{B} = \frac{1}{2}(B+C)$. The relevant energy gaps are thus multiples of $4A$, yielding the period of $1/4A \approx 304$ ps in $\langle \cos^2 \theta \rangle$.

For the stronger laser pulse, the nuclear-quadrupole interactions had a much weaker impact on the post-pulse rotational dynamics. Generally, it led to a loss of the peak alignment over time instead of qualitatively altering the dynamics[29] (see Fig. 5). An exception of this primarily destructive effect of the quadrupole coupling is found at certain alignment peaks of 1,2-DIB, e.g., $t = 5.17$ ns, where $\langle \cos^2 \theta \rangle$ with quadrupole coupling is slightly larger than without. We attribute this constructive effect of the quadrupole coupling to the hyperfine splittings of some low-energy rotational states that cause a change in the amplitude of $\langle \cos^2 \theta \rangle$ similar to the weak laser intensity regime, Fig. 2(c). Overall, the weak impact of the quadrupole interactions is a result of increasingly uniform hyperfine splitting patterns at higher rotational excitations, as previously shown for I$_2$ and 1,4-DIB.[29]

The FFTs of the post-pulse alignment for IB and 1,3-DIB are shown in Figs. 6(c) and 6(d). The stronger-intensity pulse creates much broader wave packets that contain multiple frequency components. For both molecules, the Fourier transforms calculated with and without quadrupole interactions are similar, especially for higher frequencies f that correspond to transitions between highly excited rotational states. Deviations occur mainly in the lower frequency range, which contributes to a slight dephasing and the corresponding decrease of the alignment at longer timescales, as noticed in Figs. 6(a) and 6(b). As for the weak laser intensity, the dephasing is more pronounced in 1,3-DIB due to the stronger mixing of less separated neighboring rotational states and generally larger number of the hyperfine components.

C. Influence of the temperature

While single-state molecular ensembles can be achieved for small molecules,[36,39–42] this is generally not feasible for larger molecules.[42–44] We thus need to understand the effect of the nuclear-quadrupole coupling at finite rotational temperatures. We computed the post-pulse impulsive alignment of thermal ensembles of IB molecules for the two laser intensities used above and the rotational temperatures $T_{\text{rot}} = 0.1$ K and $T_{\text{rot}} = 0.3$ K. Such thermal ensembles are comparable[45] to state selected molecular ensembles[39,42,46] and represent conditions that are experimentally achievable.

The alignment of the thermal ensembles is shown in Fig. 7. Without quadrupole interactions, $\langle \cos^2 \theta \rangle$ shows revival features with a decreased degree of alignment as compared to $T_{\text{rot}} = 0$ K, which is due to the influence of 32 (130) initially populated excited states with up to $J = 3$ ($J = 5$) for $T_{\text{rot}} = 0.1$ K ($T_{\text{rot}} = 0.3$ K). As for $T_{\text{rot}} = 0$ K, the quadrupole-coupling effects are stronger at the weaker field intensity $I_0 = 10^{11}$ W/cm^2, see Fig. 7(a). For this laser intensity, a periodic increase of the amplitude of $\langle \cos^2 \theta \rangle$ as observed for $T_{\text{rot}} = 0$ K in Fig. 2(a) is not present. At a stronger intensity $I_0 = 10^{12}$ W/cm^2, the effect of the quadrupole coupling is essentially negligible until the first full revival [see Figs. 7(b) and 7(d)]. Shortly thereafter, the quadrupole interaction starts to manifest itself, reducing the overall degree of alignment.
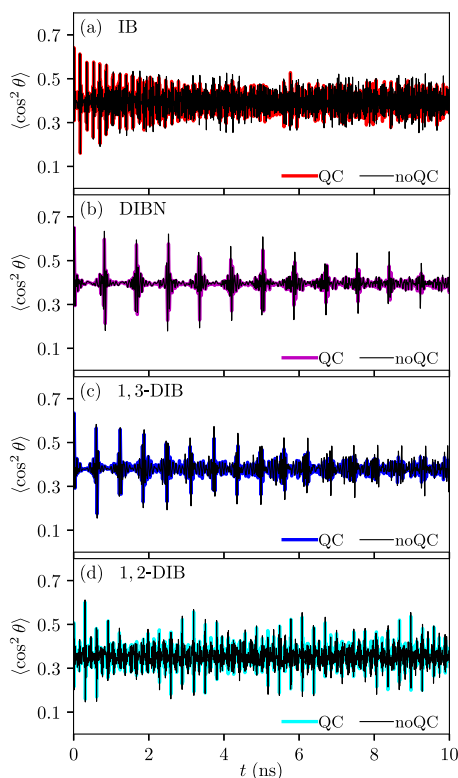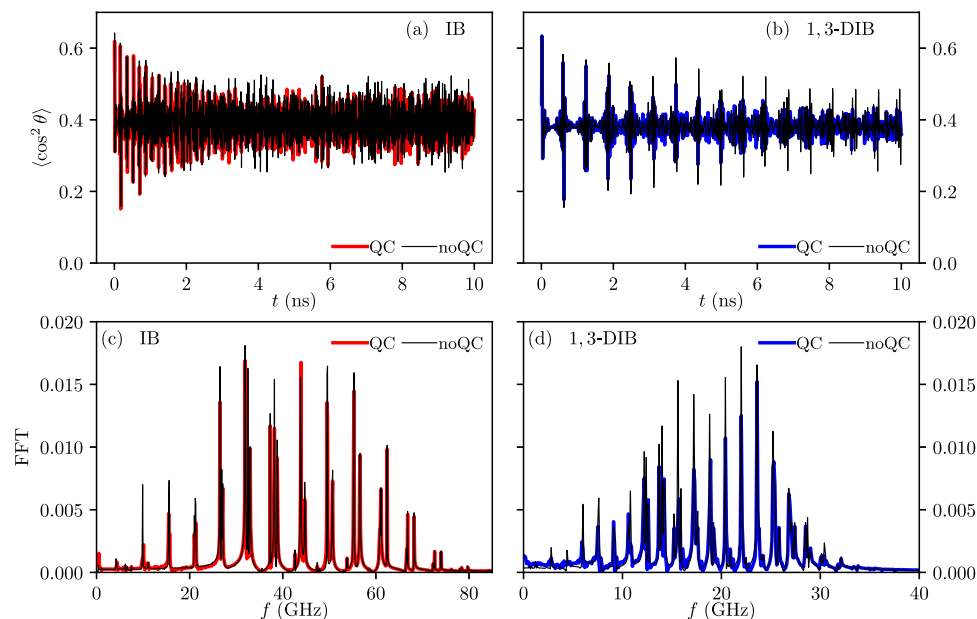
18 November 2024 12:40:21

FIG. 6. Impulsive alignment for $I_0 = 10^{12}$ W/cm^2 with (QC) and without (noQC) nuclear-quadrupole coupling for the initial states (a) $|5/2, 0_{00}, 1/2\rangle$ of IB and (b) $|0, 0_{00}, 0\rangle$ of 1,3-DIB. (c, d) Fast-Fourier transforms of $\langle\cos^2\theta\rangle$ dynamics of the dynamics in (a) and (b).

To account for the nuclear-quadrupole effect in thermal ensembles of different molecular species, we additionally computed the alignment dynamics of the excited rotational state $|2_{12}\rangle$ of 1,2-DIB (see Fig. 8). We compared the average rigid-rotor alignment over all possible M_J values of the initial state to the average result obtained for all initial hyperfine states $|F, \tilde{2}_{\bar{1}\bar{2}}, n, M\rangle$. As for the rotational ground state, the effect of the quadrupole coupling is stronger for weaker intensity laser fields. For $I_0 = 10^{12}$ W/cm^2 [Fig. 8(b)], the effect is still more pronounced than for T$_{rot}$ = 0 K in Fig. 2(d). This can be attributed to the nuclear-quadrupole interactions strongly mixing the rotational states $|2_{12}\rangle$ and $|2_{02}\rangle$, which are not coupled by the polarizability interaction. This mixing led to significant
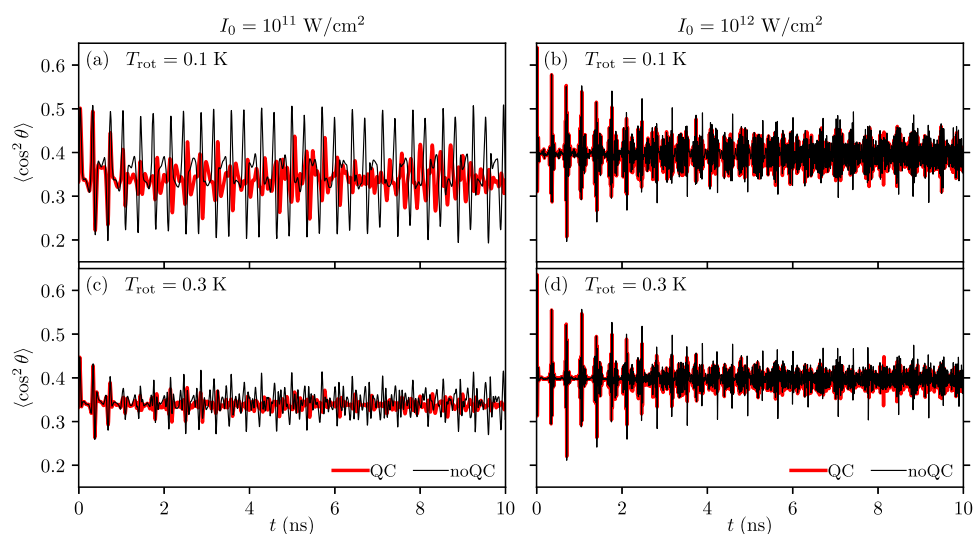

FIG. 7. Impulsive alignment of a thermal ensemble of IB molecules induced by laser pulses with τ_{FWHM} = 1 ps, including and neglecting the quadrupole coupling (QC and noQC) for [(a) and (b)] T$_{rot}$ = 0.1 K and [(c) and (d)] T$_{rot}$ = 0.3 K. (a) and (c) show the results for $I_0 = 10^{11}$ W/cm^2 and [(b) and (d)] for $I_0 = 10^{12}$ W/cm^2.
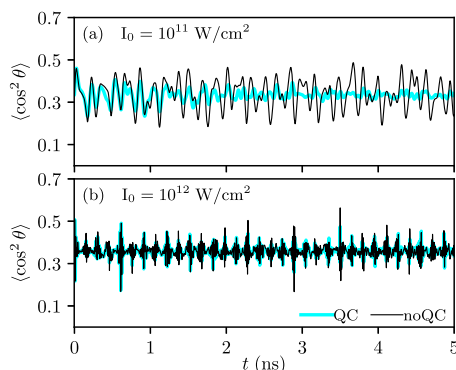
FIG. 8. Impulsive alignment averaged over the initial states $|2_{12}, M_J\rangle$ of 12-DIB induced by 1 ps laser pulses with (a) $I_0 = 10^{11}$ W/cm^2 and (b) $I_0 = 10^{12}$ W/cm^2. The alignment is shown including (QC) and neglecting the nuclear quadrupole coupling (noQC).

contributions of basis states $|F, 2_{02}, I, M\rangle$ in the initial wave functions $|F, \tilde{2}_{\tilde{1}\tilde{2}}, n, M\rangle$, modifying the dynamics even before the laser field was applied. After the interaction with the laser pulse, we find significant populations of hyperfine states belonging to rotational states that are otherwise not excited when the quadrupole coupling is neglected.

We thus conclude that for finite-temperature molecular beams, the influence of the nuclear-quadrupole interaction generally decreases with increasing the laser intensity. This is further strengthened by our previous analysis of the excited state rotational dynamics of I_2 and 1,4-DIB.[29] However, the hyperfine interactions can have a significant impact on the dynamics of some excited initial states and cannot be neglected even on a time scale where they do not affect the alignment for $T_{rot} = 0$ K.

IV. SUMMARY AND CONCLUSIONS

We presented a computational analysis of the post-pulse alignment dynamics of asymmetric top molecules with strong nuclear-quadrupole interactions. We focused on differences in the hyperfine interactions due to different chemical structures of the molecules. We showed that the interplay of hyperfine energy shifts and rotational energy level spacings is a deciding factor for the extent to which the coupling affects the post-pulse alignment. For all molecules analyzed in the present work and in previous studies,[28,29] we observed that the influence of the quadrupole coupling becomes small when the field-dressed dynamics is dominated by excited rotational states. Due to the variety of molecules considered, we expect that this observation is general and that pushing the population into highly excited rotational states is advantageous for minimizing the dephasing due to nuclear-quadrupole coupling.

While we could not find any significant enhancement of the degree of alignment due to the nuclear-quadrupole effects, coherent-control strategies could exploit the additional degrees of freedom to obtain larger degrees of alignment than without the nuclear spins.

Although not explicitly studied, we assume that the effects of nuclear spins on molecular orientation dynamics will be similar, i.e., with significant nuclear-spin effects only in low-energy-state rotational wavepackets.

We point out that while nuclear-quadrupole interactions pose difficulties in achieving strong field-free alignment, their effect on the rotational dynamics might be exploited to probe nuclear or electronic excitations that alter the nuclear spins and quadrupole momenta as well as electric field gradients. The sensitivity of the alignment to the hyperfine energy level structures of low-energy rotational states may thus be viewed as an opportunity rather than a disadvantage.

AUTHOR DECLARATIONS

Conflict of Interest

The authors have no conflicts to disclose.

Author Contributions

Linda V. Thesing: Conceptualization (equal); Data curation (equal); Investigation (equal); Methodology (equal); Software (equal); Visualization (equal); Writing – original draft (equal); Writing – review & editing (equal). **Andrey Yachmenev**: Conceptualization (equal); Formal analysis (equal); Funding acquisition (equal); Investigation (equal); Methodology (equal); Software (equal); Supervision (equal); Validation (equal); Writing – review & editing (equal). **Rosario González-Férez**: Conceptualization (equal); Formal analysis (equal); Funding acquisition (equal); Investigation (equal); Methodology (equal); Project administration (equal); Software (equal); Supervision (equal); Validation (equal); Writing – review & editing (equal). **Jochen Küpper**: Conceptualization (equal); Funding acquisition (equal); Investigation (equal); Methodology (equal); Project administration (equal); Resources (equal); Software (equal); Supervision (equal); Validation (equal); Writing – review & editing (equal).

DATA AVAILABILITY

The data that support the findings of this study are available from the corresponding author upon reasonable request.

APPENDIX A: MOLECULAR PARAMETERS

The rotational constants, asymmetry parameters $\kappa = (2B - A - C)/(A - C)$, and elements of the polarizability and EFG tensors

of the iodine and bromine nuclei in the principle axes of the inertia frame are listed in Table I. Except for IB, the rotational constants were computed from the equilibrium geometry obtained using density functional theory (DFT) with the B3LYP functional and the def2-QZVPP basis set.[48,49] The effective core potential def2-ECP[50] was used for the iodine atoms. The electric field gradient and polarizability tensors of DIBN, 1,3-DIB, and 1,2-DIB were calculated at the DFT/B3LYP level of theory using the all-electron scalar relativistic Douglas–Kroll–Hess Hamiltonian[51] with the DKH-def2-TZVP basis set.[52,53] All electronic structure calculations were carried out with the quantum-chemistry package ORCA.[54,55] For IB, we used the experimental nuclear-quadrupole coupling constants[47] $\chi_{aa} = -1892.039$ MHz, $\chi_{bb} = 978.816$ MHz, and $\chi_{cc} = 913.222$ MHz instead of a calculated electric field gradient and quadrupole moment. The molecule-fixed frame (x, y, z) is defined by the principle axes of inertia so that the z axis is parallel to the most polarizable axis or, in the case of DIBN, forms the smallest possible angle $(\approx 5°)$ with it. The z axis is thus chosen parallel to the a axis for IB, DIBN, 1,3-DIB, and 1,3-bromoiodobenzene and to the b axis for 1,2-DIB.

APPENDIX B: MATRIX REPRESENTATION OF THE HAMILTONIAN

To obtain the eigenstates of H_{mol}, we first solved the time-independent Schrödinger equation for H_{rot}, yielding the rigid-rotor energy levels and eigenstates $|J_{K_a K_c}, M_J\rangle$. Here, M_J is the eigenvalue of $\hat{J}_Z$ and $K_{a,c}$ are associated with the projections $\hat{J}_{a,c}$ and are good quantum numbers in the prolate and oblate symmetric top cases, respectively. The matrix representation of H_{mol} was then constructed in the coupled basis[56,57] $|F, J_{K_a K_c}, I, M\rangle$, M being the eigenvalue of $\hat{F}_Z$. The field-free energies and eigenstates $|F, \tilde{J}_{\tilde{K}_a \tilde{K}_c}, n, M\rangle$ were computed by numerically solving the associated time-independent Schrödinger equation. Here, $n = 1, 2, \ldots$ is an index labeling state with the same F, and the approximate quantum numbers $\tilde{J}$, $\tilde{K}_a$, and $\tilde{K}_c$ were assigned according to the coupled basis state $|F, J_{K_a K_c}, I, M\rangle$ with the largest contribution to the given eigenstate. For IB, the nuclear spin quantum number $I = I_1$ remains a good quantum number. The matrix elements of the polarizability element α_{ZZ} are known analytically[56] in the basis $|F, J_{K_a K_c}, I, M\rangle$ and can be transformed easily into the field-free eigenbasis.[28]

REFERENCES

[1]R. Altkorn, R. N. Zare, and C. H. Greene, "Depolarization of optically prepared molecules by two randomly oriented spins," Mol. Phys. 55, 1–9 (1985).

[2]C. Yan and A. C. Kummel, "Effect of hyperfine depolarization upon creation and detection of alignment in free-jet expansions via selective photodissociation," J. Chem. Phys. 98, 6869–6882 (1993).

[3]T. A. Cool and N. Hemmi, "Hyperfine polarization quantum beats in cyanogen," J. Chem. Phys. 103, 3357–3366 (1995).

[4]J. Zhang, C. W. Riehn, M. Dulligan, and C. Wittig, "An experimental study of HF photodissociation: Spin-orbit branching ratio and infrared alignment," J. Chem. Phys. 104, 7027–7035 (1996).

[5]E. R. Wouters, L. D. Siebbeles, K. L. Reid, B. Buijsse, and W. J. van der Zande, "Observation of fine structure and hyperfine structure depolarization in the photofragment anisotropy in triplet H_2," Chem. Phys. 218, 309–323 (1997).

[6]D. Sofikitis, L. Rubio-Lago, M. R. Martin, D. J. Ankeny Brown, N. C.-M. Bartlett, A. J. Alexander, R. N. Zare, and T. P. Rakitzis, "Optical control of

ground-state atomic orbital alignment: $Cl(^2P_{3/2})$ atoms from $HCl(v = 2, j = 1)$ photodissociation," J. Chem. Phys. 127, 144307 (2007).

[7]N. C.-M. Bartlett, D. J. Miller, R. N. Zare, A. J. Alexander, D. Sofikitis, and T. P. Rakitzis, "Time-dependent depolarization of aligned HD molecules," Phys. Chem. Chem. Phys. 11, 142–147 (2009).

[8]N. C.-M. Bartlett, J. Jankunas, R. N. Zare, and J. A. Harrison, "Time-dependent depolarization of aligned D_2 caused by hyperfine coupling," Phys. Chem. Chem. Phys. 12, 15689–15694 (2010).

[9]K. Grygoryeva, J. Rakovský, O. Votava, and M. Fárník, "Imaging of rotational wave-function in photodissociation of rovibrationally excited HCl molecules," J. Chem. Phys. 147, 013901 (2017).

[10]J. C. H. Spence and H. N. Chapman, "The birth of a new field," Philos. Trans. R. Soc., B 369, 20130309 (2014).

[11]J. Küpper, S. Stern, L. Holmegaard, F. Filsinger, A. Rouzée, A. Rudenko, P. Johnsson, A. V. Martin, M. Adolph, A. Aquila, S. Bajt, A. Barty, C. Bostedt, J. Bozek, C. Caleman, R. Coffee, N. Coppola, T. Delmas, S. Epp, B. Erk, L. Foucar, T. Gorkhover, L. Gumprecht, A. Hartmann, R. Hartmann, G. Hauser, P. Holl, A. Hömke, N. Kimmel, F. Krasniqi, K.-U. Kühnel, J. Maurer, M. Messerschmidt, R. Moshammer, C. Reich, B. Rudek, R. Santra, I. Schlichting, C. Schmidt, S. Schorb, J. Schulz, H. Soltau, J. C. H. Spence, D. Starodub, L. Strüder, J. Thøgersen, M. J. J. Vrakking, G. Weidenspointner, T. A. White, C. Wunderer, G. Meijer, J. Ullrich, H. Stapelfeldt, D. Rolles, and H. N. Chapman, "X-ray diffraction from isolated and strongly aligned gas-phase molecules with a free-electron laser," Phys. Rev. Lett. 112, 083002 (2013); arXiv:1307.4577 [physics].

[12]J. Yang, X. Zhu, T. J. A. Wolf, Z. Li, J. P. F. Nunes, R. Coffee, J. P. Cryan, M. Gühr, K. Hegazy, T. F. Heinz, K. Jobe, R. Li, X. Shen, T. Veccione, S. Weathersby, K. J. Wilkin, C. Yoneda, Q. Zheng, T. J. Martínez, M. Centurion, and X. Wang, "Imaging CF_3I conical intersection and photodissociation dynamics with ultrafast electron diffraction," Science 361, 64–67 (2018).

[13]M. S. Hunter, C. H. Yoon, H. DeMirci, R. G. Sierra, E. H. Dao, R. Ahmadi, F. Aksit, A. L. Aquila, H. Ciftci, S. Guillet, M. J. Hayes, T. J. Lane, M. Liang, U. Lundström, J. E. Koglin, P. Mgbam, Y. Rao, L. Zhang, S. Wakatsuki, J. M. Holton, and S. Boutet, "Selenium single-wavelength anomalous diffraction de novo phasing using an x-ray-free electron laser," Nat. Commun. 7, 13388 (2016).

[14]A. Barty, J. Küpper, and H. N. Chapman, "Molecular imaging using x-ray free-electron lasers," Annu. Rev. Phys. Chem. 64, 415–435 (2013).

[15]L. Christensen, J. H. Nielsen, C. B. Brandt, C. B. Madsen, L. B. Madsen, C. S. Slater, A. Lauer, M. Brouard, M. P. Johansson, B. Shepperson, and H. Stapelfeldt, "Dynamic Stark control of torsional motion by a pair of laser pulses," Phys. Rev. Lett. 113, 073005 (2014).

[16]R. D. Miller, "Mapping atomic motions with ultrabright electrons: The chemists' gedanken experiment enters the lab frame," Annu. Rev. Phys. Chem. 65, 583–604 (2014).

[17]H. Stapelfeldt and T. Seideman, "*Colloquium*: Aligning molecules with strong laser pulses," Rev. Mod. Phys. 75, 543–557 (2003).

[18]C. P. Koch, M. Lemeshko, and D. Sugny, "Quantum control of molecular rotation," Rev. Mod. Phys. 91, 035005 (2019).

[19]T. Seideman, "Revival structure of aligned rotational wave packets," Phys. Rev. Lett. 83, 4971–4974 (1999).

[20]F. Rosca-Pruna and M. J. J. Vrakking, "Revival structures in picosecond laser-induced alignemnt of I_2 molecules. II. Numerical modeling," J. Chem. Phys. 116, 6579 (2002).

[21]E. Hamilton, T. Seideman, T. Ejdrup, M. D. Poulsen, C. Z. Bisgaard, S. S. Viftrup, and H. Stapelfeldt, "Alignment of symmetric top molecules by short laser pulses," Phys. Rev. A 72, 043402 (2005).

[22]T. Seideman, "On the dynamics of rotationally broad, spatially aligned wave packets," J. Chem. Phys. 115, 5965 (2001).

[23]J. Underwood, M. Spanner, M. Ivanov, J. Mottershead, B. Sussman, and A. Stolow, "Switched wave packets: A route to nonperturbative quantum control," Phys. Rev. Lett. 90, 223001 (2003).

[24]J. Underwood, B. Sussman, and A. Stolow, "Field-free three dimensional molecular axis alignment," Phys. Rev. Lett. 94, 143002 (2005).

[25]A. Goban, S. Minemoto, and H. Sakai, "Laser-field-free molecular orientation," Phys. Rev. Lett. 101, 013001 (2008).

[26] A. Chatterley, E. T. Karamatskos, C. Schouder, L. Christiansen, A. V. Jörgensen, T. Mullins, J. Küpper, and H. Stapelfeldt, "Communication: Switched wave packets with spectrally truncated chirped pulses," J. Chem. Phys. **148**, 221105 (2018); arXiv:1803.03953 [physics].

[27] E. F. Thomas, A. A. Søndergaard, B. Shepperson, N. E. Henriksen, and H. Stapelfeldt, "Hyperfine-structure-induced depolarization of impulsively aligned I_2 molecules," Phys. Rev. Lett. **120**, 163202 (2018); arXiv:1804.04416 [physics].

[28] A. Yachmenev, L. V. Thesing, and J. Küpper, "Laser-induced dynamics of molecules with strong nuclear quadrupole coupling," J. Chem. Phys. **151**, 244118 (2019); arXiv:1910.13275 [physics].

[29] L. V. Thesing, A. Yachmenev, R. González-Férez, and J. Küpper, "The effect of nuclear-quadrupole coupling in the laser-induced alignment of molecules," J. Phys. Chem. A **124**, 2225–2230 (2020); arXiv:1911.12270 [physics].

[30] P. Pyykkö, "Year-2008 nuclear quadrupole moments," Mol. Phys. **106**, 1965–1974 (2008).

[31] A. Owens and A. Yachmenev, "RichMol: A general variational approach for rovibrational molecular dynamics in external electric fields," J. Chem. Phys. **148**, 124102 (2018); arXiv:1802.07603 [physics].

[32] W. Gordy and R. L. Cook, *Microwave Molecular Spectra*, 3rd ed. (John Wiley & Sons, New York, 1984).

[33] F. Rosca-Pruna and M. J. J. Vrakking, "Experimental observation of revival structures in picosecond laser-induced alignment of I_2," Phys. Rev. Lett. **87**, 153902 (2001).

[34] L. Holmegaard, S. S. Viftrup, V. Kumarappan, C. Z. Bisgaard, H. Stapelfeldt, E. Hamilton, and T. Seideman, "Control of rotational wave-packet dynamics in asymmetric top molecules," Phys. Rev. A **75**, 051403 (2007).

[35] S. Trippel, T. Mullins, N. L. M. Müller, J. S. Kienitz, J. J. Omiste, H. Stapelfeldt, R. González-Férez, and J. Küpper, "Strongly driven quantum pendulum of the carbonyl sulfide molecule," Phys. Rev. A **89**, 051401(R) (2014); arXiv:1401.6897 [quant-ph].

[36] E. T. Karamatskos, S. Raabe, T. Mullins, A. Trabattoni, P. Stammer, G. Goldsztejn, R. R. Johansen, K. Długołęcki, H. Stapelfeldt, M. J. J. Vrakking, S. Trippel, A. Rouzée, and J. Küpper, "Molecular movie of ultrafast coherent rotational dynamics of OCS," Nat. Commun. **10**, 3364 (2019); arXiv:1807.01034 [physics].

[37] M. D. Poulsen, E. Peronne, H. Stapelfeldt, C. Z. Bisgaard, S. Viftrup, E. Hamilton, and T. Seideman, "Nonadiabatic alignment of asymmetric top molecules: Rotational revivals," J. Chem. Phys. **121**, 783–791 (2004).

[38] A. Rouzee, S. Guerin, V. Boudon, B. Lavorel, and O. Faucher, "Field-free one-dimensional alignment of ethylene molecule," Phys. Rev. A **73**, 033418–033419 (2006).

[39] Y.-P. Chang, D. A. Horke, S. Trippel, and J. Küpper, "Spatially-controlled complex molecules and their applications," Int. Rev. Phys. Chem. **34**, 557–590 (2015); arXiv:1505.05632 [physics].

[40] J. H. Nielsen, P. Simesen, C. Z. Bisgaard, H. Stapelfeldt, F. Filsinger, B. Friedrich, G. Meijer, and J. Küpper, "Stark-selected beam of ground-state OCS molecules characterized by revivals of impulsive alignment," Phys. Chem. Chem. Phys. **13**, 18971–18975 (2011); arXiv:1105.2413 [physics].

[41] D. A. Horke, Y.-P. Chang, K. Długołęcki, and J. Küpper, "Separating para and ortho water," Angew. Chem., Int. Ed. **53**, 11965–11968 (2014); arXiv:1407.2056 [physics].

[42] S. Y. T. van de Meerakker, H. L. Bethlem, N. Vanhaecke, and G. Meijer, "Manipulation and control of molecular beams," Chem. Rev. **112**, 4828–4878 (2012).

[43] K. Wohlfart, F. Grätz, F. Filsinger, H. Haak, G. Meijer, and J. Küpper, "Alternating-gradient focusing and deceleration of large molecules," Phys. Rev. A **77**, 031404(R3) (2008); arXiv:0803.0650 [physics].

[44] H. L. Bethlem, M. R. Tarbutt, J. Küpper, D. Carty, K. Wohlfart, E. A. Hinds, and G. Meijer, "Alternating gradient focusing and deceleration of polar molecules," J. Phys. B: At., Mol. Opt. Phys. **39**, R263–R291 (2006); arXiv:0604020 [physics].

[45] L. V. Thesing, J. Küpper, and R. González-Férez, "Time-dependent analysis of the mixed-field orientation of molecules without rotational symmetry," J. Chem. Phys. **146**, 244304 (2017); arXiv:1705.03225 [physics].

[46] F. Filsinger, G. Meijer, H. Stapelfeldt, H. N. Chapman, and J. Küpper, "State- and conformer-selected beams of aligned and oriented molecules for ultrafast diffraction studies," Phys. Chem. Chem. Phys. **13**, 2076–2087 (2011); arXiv:1009.0871 [physics].

[47] J. L. Neill, S. T. Shipman, L. Alvarez-Valtierra, A. Lesarri, Z. Kisiel, and B. H. Pate, "Rotational spectroscopy of iodobenzene and iodobenzene–neon with a direct digital 2–8 GHz chirped-pulse Fourier transform microwave spectrometer," J. Mol. Spectrosc. **269**, 21–29 (2011).

[48] F. Weigend, F. Furche, and R. Ahlrichs, "Gaussian basis sets of quadruple zeta valence quality for atoms H–Kr," J. Chem. Phys. **119**, 12753–12762 (2003).

[49] F. Weigend and R. Ahlrichs, "Balanced basis sets of split valence, triple zeta valence and quadruple zeta valence quality for H to Rn: Design and assessment of accuracy," Phys. Chem. Chem. Phys. **7**, 3297 (2005).

[50] K. A. Peterson, D. Figgen, E. Goll, H. Stoll, and M. Dolg, "Systematically convergent basis sets with relativistic pseudopotentials. II. Small-core pseudopotentials and correlation consistent basis sets for the post-d group 16–18 elements," J. Chem. Phys. **119**, 11113–11123 (2003).

[51] F. Neese, A. Wolf, T. Fleig, M. Reiher, and B. A. Hess, "Calculation of electric-field gradients based on higher-order generalized Douglas–Kroll transformations," J. Chem. Phys. **122**, 204107 (2005).

[52] F. E. Jorge, A. Canal Neto, G. G. Camiletti, and S. F. Machado, "Contracted Gaussian basis sets for Douglas–Kroll–Hess calculations: Estimating scalar relativistic effects of some atomic and molecular properties," J. Chem. Phys. **130**, 064108 (2009).

[53] C. Campos and F. Jorge, "Triple zeta quality basis sets for atoms Rb through Xe: Application in CCSD(T) atomic and molecular property calculations," Mol. Phys. **111**, 167–173 (2012).

[54] F. Neese, "The ORCA program system," WIREs Comput. Mol. Sci. **2**, 73–78 (2011).

[55] F. Neese, "Software update: The ORCA program system, version 4.0," WIREs Comput. Mol. Sci. **8**, e1327 (2017).

[56] R. L. Cook and F. C. de Lucia, "Application of the theory of irreducible tensor operators to molecular hyperfine structure," Am. J. Phys. **39**, 1433–1454 (1971).

[57] A. Yachmenev and J. Küpper, "Communication: General variational approach to nuclear-quadrupole coupling in rovibrational spectra of polyatomic molecules," J. Chem. Phys. **147**, 141101 (2017); arXiv:1709.08558 [physics].

18 November 2024 12:40:21